1521-0111/94/5/1256–1269$35.00
MOLECULAR PHARMACOLOGY
Copyright © 2018 by The American Society for Pharmacology and Experimental Therapeutics
https://doi.org/10.1124/mol.118.113076
Mol Pharmacol 94:1256–1269, November 2018

The Novel Activity of Carbamazepine as an Activation Modulator Extends from $Na_V1.7$ Mutations to the $Na_V1.8$-S242T Mutant Channel from a Patient with Painful Diabetic Neuropathy

Chongyang Han, Andreas C. Themistocleous, Mark Estacion, Fadia B. Dib-Hajj, Iulia Blesneac, Lawrence Macala, Carl Fratter, David L. Bennett, Stephen G. Waxman, and Sulayman D. Dib-Hajj

Department of Neurology and Center for Neuroscience and Regeneration Research, Yale University School of Medicine, New Haven, Connecticut (C.H., M.E., F.B.D.-H., L.M., S.G.W., S.D.D.-H.); Center for restoration of Nervous System Function, Veterans Affairs Medical Center, West Haven, Connecticut (C.H., M.E., F.B.D.-H., L.M., S.G.W., S.D.D.-H.); Nuffield Department of Clinical Neurosciences, University of Oxford, Oxford, United Kingdom (A.C.T., I.B., D.L.B.); Brain Function Research Group, School of Physiology, Faculty of Health Sciences, University of the Witwatersrand, Johannesburg, South Africa (A.C.T.); and Oxford Medical Genetics Laboratories, Oxford University Hospitals NHS Foundation Trust, Oxford, United Kingdom (C.F.)

Received May 22, 2018; accepted August 20, 2018

ABSTRACT

Neuropathic pain in patients carrying sodium channel gain-of-function mutations is generally refractory to pharmacotherapy. However, we have shown that pretreatment of cells with clinically achievable concentration of carbamazepine (CBZ; 30 μM) depolarizes the voltage dependence of activation in some $Na_V1.7$ mutations such as S241T, a novel CBZ mode of action of this drug. CBZ reduces the excitability of dorsal root ganglion (DRG) neurons expressing $Na_V1.7$-S241T mutant channels, and individuals carrying the S241T mutation respond to treatment with CBZ. Whether the novel activation-modulating activity of CBZ is specific to $Na_V1.7$, and whether this pharmacogenomic approach can be extended to other sodium channel subtypes, are not known. We report here the novel $Na_V1.8$-S242T mutation, which corresponds to the $Na_V1.7$-S241T mutation, in a patient with neuropathic pain and diabetic peripheral neuropathy. Voltage-clamp recordings demonstrated hyperpolarized and accelerated activation of $Na_V1.8$-S242T. Current-clamp recordings showed that $Na_V1.8$-S242T channels render DRG neurons hyperexcitable. Structural modeling shows that despite a substantial difference in the primary amino acid sequence of $Na_V1.7$ and $Na_V1.8$, the S242 ($Na_V1.8$) and S241 ($Na_V1.7$) residues have similar position and orientation in the domain I S4-S5 linker of the channel. Pretreatment with a clinically achievable concentration of CBZ corrected the voltage dependence of activation of $Na_V1.8$-S242T channels and reduced DRG neuron excitability as predicted from our pharmacogenomic model. These findings extend the novel activation modulation mode of action of CBZ to a second sodium channel subtype, $Na_V1.8$.

Introduction

Sodium channels underlie the initiation and propagation of action potentials, and gain-of-function mutations of sodium channels have been linked to a spectrum of human pain disorders (Dib-Hajj et al., 2010, 2015, 2017; Bennett and Woods, 2014). The $Na_V1.8$-tetrodotoxin-resistant (TTX-R) sodium channel is preferentially expressed in dorsal root ganglion (DRG) neurons (Akopian et al., 1996), has been shown to contribute most of the sodium current underlying the rising phase of action potentials (Renganathan et al., 2001; Blair and Bean, 2002), and supports high-frequency firing in response to depolarization (Renganathan et al., 2001). $Na_V1.8$ has been linked to pain in a rat model of diabetes (Mert and Gunes, 2012). Electrophysiological recordings have shown increased TTX-R sodium currents from small-diameter DRG neurons from diabetic rats, accompanied by shifts in the voltage dependence of activation and steady-state fast-inactivation of the channel (Hong et al., 2004). The exposure of DRG neurons to methylglyoxal, a glucose metabolite that accumulates in diabetes, has been shown to depolarize voltage

S.G.W. and S.D.D.-H. were supported by Center Grant [B9253-C] from the Rehabilitation Research Service, Department of Veterans Affairs, USA, and a gift from The Erythromelalgia Association. D.L.B. is a Wellcome Senior Clinical Scientist [Grant 202747/Z/16/Z]. A.C.T., I.B., and D.L.B. are members of the DOLORisk consortium funded by the European Commission Horizon 2020 [ID633491]. A.C.T. and D.L.B. are members of the International Diabetic Neuropathy Consortium, the Novo Nordisk Foundation [Grant NNF14SA0006]. The Center for Neuroscience and Regeneration Research is a Collaboration of the Paralyzed Veterans of America with Yale University. No potential conflicts of interest relevant to this article are reported.
https://doi.org/10.1124/mol.118.113076.

ABBREVIATIONS: CBZ, carbamazepine; CI, confidence interval; D, domain; DMSO, dimethylsulfoxide; DPN, diabetic peripheral neuropathy; DRG, dorsal root ganglion; *G*, conductance; *I*, inward current; IEM, inherited erythromelalgia; IENFD, intraepidermal nerve fiber density; MAF, minimal allele frequency; MOE, Molecular Operating Environment; Na_V, voltage-gated sodium channel; QST, quantitative sensory testing; S242T, $Na_V1.8$-S242T; TCSS, Toronto Clinical Scoring System; TTX-R, tetrodotoxin-resistant; $V_{1/2}$, half-maximal potential; $V_{1/2,act}$, potential at which activation is half maximal; WT, $Na_V1.8$-WT.

MOLECULAR PHARMACOLOGY
Downloaded from molpharm.aspetjournals.org at ASPET Journals on January 13, 2020

dependence of the fast inactivation of $Na_V1.8$ and produce a reduction in rheobase, which is consistent with a contribution of $Na_V1.8$ to the hyperexcitability of these neurons in diabetic models (Bierhaus et al., 2012). Recently, gain-of-function $Na_V1.8$ mutations have been identified in patients with painful small fiber neuropathy, including subjects with diabetic peripheral neuropathy (DPN) (Faber et al., 2012b; Huang et al., 2013; Han et al., 2014).

Although carbamazepine (CBZ), a Food and Drug Administration–approved antiepileptic Na_V blocker, is not recommended as a first-line treatment of neuropathic pain (Finnerup et al., 2015), it is still used clinically in selected patients with some success. Importantly, CBZ has demonstrated effectiveness in the treatment of the pain disorder trigeminal neuralgia (Maarbjerg et al., 2017). The classic action of CBZ is to inhibit Na_Vs in a voltage- and use-dependent manner (Tanelian and Brose, 1991; Kuo et al., 1997; Kuo, 1998; Yang et al., 2010). Although CBZ action on Na_V is indisputable, especially at clinically achievable concentrations, it has been shown to also act on other ion channels and receptors (Ambrósio et al., 2002) that might contribute to its analgesic effect. Recently, we have demonstrated a novel action of CBZ as an activation modulator of mutant $Na_V1.7$ channels, in which clinically achievable concentrations of CBZ (10–30 μM) depolarize the voltage dependence of activation; plasma levels in patients with epilepsy treated with CBZ range from 0.92 to 16 mg/l, which corresponds to 3.89–67.5 μM (Breton et al., 2005). CBZ (10–30 μM) depolarizes the activation of mutant $Na_V1.7$ channels including $Na_V1.7$-S241T (Yang et al., 2012), $Na_V1.7$-V400M (Fischer et al., 2009), and $Na_V1.7$-I234T (Yang et al., 2018), but not wild-type $Na_V1.7$, and reduces the excitability of DRG neurons that express these mutant $Na_V1.7$ channels (Yang et al., 2012, 2018; Geha et al., 2016). Open-label use of CBZ was reported to be beneficial in treating inherited erythromelalgia (IEM) patients carrying the $Na_V1.7$-V400M mutation (Fischer et al., 2009) and $Na_V1.7$-I234T mutation (Meijer et al., 2014). In a placebo-controlled, double-blind clinical study, we showed that CBZ (plasma concentration of 3.6–6.0 mg/l, which corresponds to 15.22–25.37 μM) was effective in treating patients with IEM carrying the $Na_V1.7$-S241T mutation (Geha et al., 2016). However, except for the pharmacogenomic targeting of $Na_V1.7$ carrying specific CBZ-responsive mutations (Fertleman et al., 2006; Fischer et al., 2009; Meijer et al., 2014; Geha et al., 2016), to date, CBZ has not been used to target other Na_V isoforms based on their primary sequence.

The identification of gain-of-function mutations in $Na_V1.8$ in individuals with painful peripheral neuropathy suggests that $Na_V1.8$ channels contribute to neuropathic pain in peripheral neuropathy (Faber et al., 2012b; Huang et al., 2013; Han et al., 2014); thus, inhibitors of this channel may have therapeutic benefits. Whether the novel mode of action of CBZ extends to other Na_Vs is not known. We describe here, in an individual with painful diabetic neuropathy a novel mutation in $Na_V1.8$, S242T. Using patch-clamp recordings, we investigated the effects of the mutation at the channel level by voltage clamp, and the effects of expressing mutant channels on the excitability of DRG neurons by current clamp. We extrapolated from studies of CBZ interaction with the homologous $Na_V1.7$-S241T mutation to ask whether the novel mechanism of action for this drug as activation modulator extends to $Na_V1.8$-S242T (referred to as S242T), and to determine whether CBZ at clinically achievable concentrations reduces the hyperexcitability of DRG neurons expressing the mutant channel. Our studies ultimately aim to determine whether the novel mode of action of CBZ is isoform specific.

Materials and Methods

Patient and Clinical Examinations. A 67-year-old male patient with diabetes was recruited as part of the Pain in Neuropathy Study (Themistocleous et al., 2016), an observational cross-sectional multicenter study approved by the National Research Ethics Service of the UK (No. 10/H0706/35). All participants signed informed consent forms, and the consent of Pain in Neuropathy Study participants (2010–2015) was made on the basis that they would not be told the result of the sequencing of Na_V genes. A detailed description of the study protocol was given previously (Themistocleous et al., 2016). Clinical assessment included clinical history, structured neurologic examination, skin biopsy to determine the intraepidermal nerve fiber density (IENFD), and quantitative sensory testing (QST).

Pain intensity was reported on an 11-point numerical rating scale, with 0 being no pain and 10 the worst pain imaginable, and pain location was indicated on a body map. The Douleur Neuropathique 4 Questionnaire (Bouhassira et al., 2005) was used as a screening tool for neuropathic pain. A comprehensive structured upper and lower limb neurologic examination was performed to detect clinical signs of a peripheral neuropathy (Kleyweg et al., 1991; Compston, 2010). The examination included the assessment of light touch, pinprick sensation, proprioception, vibration perception, deep-tendon reflexes, muscle bulk, and motor power. The clinical findings were quantified with the Toronto Clinical Scoring System (TCSS) (Bril and Perkins, 2002). TCSS is a screening tool for DPN and correlates with diabetic neuropathy severity.

The determination of IENFD followed the European Federation of Neurologic Societies/Peripheral Nerve Society Guideline on the utilization of skin biopsy (Lauria et al., 2010). QST is a measure of sensory perception in response to a given stimulus and can be used to demonstrate abnormalities in sensory function. QST was performed over the dorsum of both feet, in line with the published protocol of the German Research Network of Neuropathic Pain (Rolke et al., 2006). Raw QST data were transformed into z-scores to normalize for age, sex, and the body location of testing (Rolke et al., 2006; Maier et al., 2010). A z-score of zero is equal to the mean of the population. A score of greater or less than 2 S.D.s from the mean indicates gain of function or loss of function, respectively. Additional drug, laboratory, and clinical investigation data were retrieved from the clinical medical records.

Sequencing of Sodium Channels. Sequencing of the coding regions of *SCN9A* (encodes $Na_V1.7$), *SCN10A* (encodes $Na_V1.8$), and *SCN11A* (encodes $Na_V1.9$) was undertaken by next-generation sequencing using the HaloPlex Target Enrichment System (Agilent Technologies, Santa Clara, CA) and the MiSeq Sequencing Platform (Illumina, Inc., San Diego, CA) after DNA extraction from blood. Variants were called using an in-house bioinformatics pipeline (further details available on request). Any variant that was both: 1) present at >1% allele frequency in the Exome Variant Database (http://evs.gs.washington.edu/EVS) or Exome Aggregation Consortium (http://exac.broadinstitute.org), and 2) not previously reported in the literature in association with painful neuropathy was considered unlikely to be pathogenic and was not investigated further. Rare variants that were present at <1% allele frequency in population databases were considered for further analysis, irrespective of whether they were previously reported in the literature in association with painful neuropathy or not. Variants of potential interest were confirmed by Sanger sequencing by capillary electrophoresis using a 3730 DNA Analyzer (Applied Biosystems, Foster City, CA). The in silico prediction of the functional effect of the variant was performed using multiple algorithms: Align GVGD (http://agvgd.hci.utah.edu/),

Downloaded from molpharm.aspetjournals.org at ASPET Journals on January 13, 2020

SIFT (http://sift.jcvi.org), and PolyPhen-2 (http://genetics.bwh.harvard.edu/pph2/).

Structural Modeling. Homology models for both the $Na_V1.8$ and $Na_V1.7$ were developed based on the recently published electric eel sodium channel structure (Yan et al., 2017) by using the homology modeler tool in Molecular Operating Environment (MOE) software (MOE, 2013.08; Chemical Computing Group ULC, Montreal, QC, Canada).

Functional Assessments of $Na_V1.8$ S242T Mutant. The *pcDNA5-GFP-2A-$Na_V1.8$* plasmid encoding enhanced green fluorescent protein and a "StopGo" 33–amino acid 2A linker upstream of the human $Na_V1.8$ ATG codon was previously described (Faber et al., 2012b; Huang et al., 2013; Han et al., 2014). The nucleotide substitution c.724T>A, which leads to the amino acid substitution Ser242Thr was introduced into the construct using QuikChange Lightning site-directed mutagenesis (Agilent Technologies).

Primary Mouse DRG Neuron Isolation and Transfection. Animal studies were approved by US Veterans Affairs West Haven Medical Center Animal Care and Use Committee. DRG neurons were isolated, as previously reported (Faber et al., 2012b; Huang et al., 2013; Han et al., 2014), from homozygous $Na_V1.8$-cre mice (4–8 weeks of age, both male and female) that lack functional endogenous $Na_V1.8$ channels. In compliance with recent National Institutes of Health guidelines and our own practice, we have used both male and female mice as the source for DRG neurons. Briefly, DRGs were harvested, incubated at 37°C for 20 minutes in complete saline solution (in mM: 137 NaCl, 5.3 KCl, 1 $MgCl_2$, 25 sorbitol, 3 $CaCl_2$, and 10 HEPES, adjusted to pH 7.2 with NaOH), containing 0.5 U/ml Liberase TM (Sigma-Aldrich, St. Louis, MO) and 0.6 mM EDTA, followed by a 15-minute incubation at 37°C in complete saline solution containing 0.5 U/ml Liberase TL (Sigma-Aldrich), 0.6 mM EDTA, and 30 U/ml papain (Worthington Biochemical, Lakewood NJ). Tissue was then centrifuged and triturated in 0.5 ml of DRG media: Dulbecco's modified Eagle's medium/F12 (1:1) with 100 U/ml penicillin, 0.1 mg/ml streptomycin (Life Technologies, Grand Island, NY), and 10% fetal bovine serum (Hyclone, Logan, UT), containing 1.5 mg/ml bovine serum albumin (low endotoxin; Sigma-Aldrich) and 1.5 mg/ml trypsin inhibitor (Sigma-Aldrich). After trituration, $Na_V1.8$-WT (referred to as WT) or S242T mutant channel constructs were transfected into DRG neurons in suspension using a Nucleofector IIS Electroporator (Lonza, Walkersville, MD) and Amaxa SCN Nucleofector reagents (VSPI-1003; Lonza). After electroporation, 100 μl of calcium-free Dulbecco's modified Eagle's medium (Lonza) was added, and cells were incubated at 37°C for 5 minutes in a 95% air/5% CO_2 (v/v) incubator to allow neurons to recover. The cell mixture was then diluted with DRG media containing 1.5 mg/ml bovine serum albumin (low endotoxin; Sigma-Aldrich) and 1.5 mg/ml trypsin inhibitor (Sigma-Aldrich), seeded onto poly-D-lysine/laminin-coated coverslips (Corning, Discovery Labware, Bedford, MA) and incubated at 37°C to allow DRG neurons to attach to the coverslips. After 40 minutes of incubation, DRG media were added to each well to a final volume of 1.0 ml. For current-clamp recording culture, medium was supplemented with 50 ng/ml mouse nerve growth factor (Alomone Laboratories, Jerusalem, Israel) and 50 ng/ml recombinant human glial cell line–derived neurotrophic factor (PeproTech, Rocky Hill, NJ), and the DRG neurons were maintained at 37°C in a 95% air/5% (v/v) CO_2 incubator for 40~48 hours before recording.

Electrophysiology and Pharmacology. Voltage-clamp and current-clamp recordings were obtained with an EPC-10 Amplifier (HEKA Electronics, Holliston, MA) from small transfected mouse DRG neurons (diameter, <25 μm) with robust green fluorescence at room temperature (~22°C), 40–48 hours after transfection, as described previously (Faber et al., 2012b; Huang et al., 2013; Han et al., 2014, 2015). As in our previous studies (Faber et al., 2012a), to minimize the variability of DRG neuron cultures prepared at different times, we carried out head-to-head comparisons of cells transfected with WT or mutant channels and cells treated with CBZ or vehicle, from cultures prepared contemporaneously by the same researcher.

Voltage-Clamp Recording from Transfected $Na_V1.8$-Null Mouse DRG Neurons. Fire-polished electrodes (1–2 MΩ) were fabricated from 1.6 mm-outer-diameter borosilicate glass micropipettes (World Precision Instruments, Sarasota, FL). The pipette potential was adjusted to zero before seal formation, and liquid junction potential was not corrected. Capacitive transients were cancelled, and voltage errors were minimized with 80%–90% series resistance compensation; cells were excluded from analysis if the predicted voltage error exceeded 4 mV. Leakage current was digitally subtracted online using hyperpolarizing control pulses, applied before the test pulse (P/6 subtraction). Currents were acquired with PatchMaster software (HEKA Electronics), 5 minutes after establishing whole-cell configuration, sampled at a rate of 50 kHz and filtered at 2.9 kHz. The pipette solution contained the following (in mM): 140 CsF, 10 NaCl, 1 EGTA, and 10 HEPES, at pH 7.3 with CsOH (adjusted to 315 mOsmol/l with dextrose). The extracellular bath solution contained the following (in mM): 70 NaCl, 70 choline chloride, 3 KCl, 1 $MgCl_2$, 1 $CaCl_2$, 10 HEPES, 5 CsCl, 20 TEA chloride, pH 7.32 with NaOH (327 mOsmol/l). TTX (0.5 μM), $CdCl_2$ (0.1 mM), and 4-aminopyridine (1 mM) were added in the bath solution to block endogenous TTX-sensitive voltage-gated sodium currents, calcium currents, and potassium currents, respectively. Endogenous $Na_V1.9$ currents were suppressed by holding the cells at −70 mV, a step that inactivates $Na_V1.9$ channels and minimizes their contribution to the TTX-R current (Cummins et al., 1999).

For current-voltage relationships, cells were held at −70 mV and stepped to a range of potentials (−70 to +40 mV in 5-mV increments) for 100 milliseconds with a 5-second interval between each sweep. Peak inward currents (I) were plotted as a function of depolarization potential to generate I-V curves. Activation curves were obtained by converting I to conductance (G) at each voltage (V) using the equation $G = I/(V - V_{rev})$, where V_{rev} is the reversal potential that was determined for each cell individually. The activation curve of each cell was then fit with Boltzmann functions in the form of $G = G_{max}/(1 + exp[(V_{1/2,act} - V)/k])$, where G_{max} is the maximal sodium G value, $V_{1/2,act}$ is the potential at which activation is half maximal, V is the test potential, and k is the slope factor. The fit parameters such as $V_{1/2,act}$ are grouped and then evaluated for significance between groups using two-tailed t tests.

Steady-state fast inactivation was achieved with a series of 500-millisecond prepulses (−90 to +10 mV in 5 mV increments), and the remaining noninactivated channels were activated by a 40-millisecond step depolarization to 0 mV. The protocol for slow-inactivation consisted of a 30-second step to potentials varying from −120 to 20 mV, followed by a 30-millisecond step to −70 mV to remove fast inactivation and a 20-millisecond step to 0 mV to elicit a test response. Peak I values obtained from steady-state fast-inactivation and slow-inactivation protocols were normalized by the maximum current amplitude for each cell and were fit with a Boltzmann equation of the form $I/I_{max} = A + (1 - A)/(1 + exp[(V - V_{1/2,inact})/k])$, where V represents the inactivating prepulse potential, and $V_{1/2,inact}$ represents the midpoint of the inactivation. The fit parameters such as inactivation $V_{1/2}$ are grouped and then evaluated for significance between groups using two-tailed t tests.

Deactivation was estimated from current decay, using a 3-millisecond short-depolarizing pulse to 0 mV followed by a 100-millisecond repolarizing pulse to potentials ranging from −110 to −20 mV in 5-mV increments, and the holding potential for deactivation was −70 mV. Deactivation kinetics were calculated by fitting the decaying currents with a single exponential function. Differences between groups are evaluated point by point using unpaired two-tailed t tests with Bonferroni correction for multiple comparisons.

Persistent currents were measured as mean amplitudes of currents recorded between 85 and 95 milliseconds after the onset of depolarization and are presented as a percentage of the maximal transient peak current. Ramp currents were elicited with slow ramp depolarization over a 600-millisecond period at 0.2 mV/ms. The amplitude of ramp current was presented as a percentage of the maximal peak current. Differences between groups are evaluated point by point

Downloaded from molpharm.aspetjournals.org at ASPET Journals on January 13, 2020

using unpaired two-tailed *t* tests with Bonferroni correction for multiple comparisons.

Current-Clamp Recording from Transfected $Na_V1.8$-Null Mouse DRG Neurons. To reduce observer bias, current-clamp recordings were performed in a blind manner where the electrophysiologist was not aware whether the neurons were transfected with wild-type or mutant channels. Electrodes had a resistance of 1–3 MΩ when filled with the pipette solution, which contained the following (in mM): 140 KCl, 0.5 EGTA, 5 HEPES, and 3 Mg-ATP, pH 7.3 with KOH (adjusted to 315 mM with dextrose). The extracellular solution contained the following (in mM): 140 NaCl, 3 KCl, 2 $MgCl_2$, 2 $CaCl_2$, and 10 HEPES, pH 7.3 with NaOH (adjusted to 320 mM with dextrose). Whole-cell configuration was obtained in voltage-clamp mode before proceeding to the current-clamp recording mode. The current threshold was determined by the first action potential elicited by a series of 200-millisecond depolarizing current injections that increased in 5-pA increments with the sweep interval of 10 seconds. Cells with stable resting membrane potentials more negative than −40 mV and overshooting action potentials (>80 mV resting membrane potential to peak) were used for additional data collection. Action potential frequency was determined by quantifying the number of action potentials elicited in response to depolarizing current injections (500 milliseconds).

CBZ Treatment. CBZ was purchased from Sigma-Aldrich, and a stock is prepared by dissolving in dimethylsulfoxide (DMSO). For pharmacology experiments, CBZ aliquots were added to produce a working solution of a clinically achievable concentration of CBZ (30 μM) (Breton et al., 2005) in 0.1% DMSO (final concentration). Cells were treated with CBZ (30 μM) or 0.1% DMSO in incomplete DRG media (without the 10% fetal bovine serum) for 30 minutes before recording, and the CBZ or DMSO concentration was maintained in the bath solution during the recording as described previously (Fischer et al., 2009; Yang et al., 2012, 2018; Geha et al., 2016). Shorter treatment periods of 2 and 5 minutes were not enough to produce a depolarizing shift in activation of $Na_V1.7$-S241T channels (data not shown), whereas a 30-minute treatment period was effective and was thus implemented in the current studies, which is consistent with prior observations on the effect of CBZ on mutant $Na_V1.7$ channels (Fischer et al., 2009; Geha et al., 2016).

Statistics. Voltage-clamp and current-clamp data were analyzed using FitMaster (HEKA Electronics) and OriginPro8.5 (OriginLab Corporation, Northampton, MA). As described above, we carried out head-to-head comparisons of cells transfected with WT or mutant channels, and of cells treated with CBZ or vehicle, from cultures prepared contemporaneously by the same researcher to minimize culture-to-culture variability. Except where noted, statistical significance was determined using an independent two-tailed *t* test with unequal variance, with Bonferroni correction for multiple comparisons when appropriate. The percentages of spontaneously firing cells were compared using the *z* test. The Mann-Whitney test was used to compare current threshold. The number of evoked action potentials between two different groups was evaluated using two-way ANOVA. All electrophysiology data are presented as the mean ± S.E.M., and error bars in the figures represent the S.E.M. A *P* value of less than 0.05 was considered statistically significant.

Results

Case History

The 67-year-old male patient had received a diagnosis of type 2 diabetes mellitus at the age of 42 years, and his recent glycated hemoglobin A1c level was 8.2%. He developed pain, paresthesia, and numbness in both of his feet 12 years prior to assessment for this study. At the time of assessment, he reported pain and paresthesia in his feet and hands. He rated pain intensity over the 24 hours before clinical assessment as 3 of 10, with a Douleur Neuropathique 4 Questionnaire score of 7 (>4 indicative of neuropathic pain). He was not taking any analgesic medication. He did not complain of autonomic symptoms. His deceased father had also suffered from painful diabetic neuropathy, but no other family members were available for segregation analysis.

Neurologic examination identified a severe length-dependent sensory neuropathy that extended to his knees and wrists bilaterally with no weakness. Deep tendon reflexes were absent at the knees and ankles bilaterally. The TCSS score was 17, which is indicative of a severe neuropathy. QST revealed bilateral hyposensitivity in relation to both thermal and mechanical detection thresholds. The IENFD assessed at 10 cm above the lateral malleolus was markedly reduced (0 fibers/mm). The clinical presentation was therefore of a severe painful sensory neuropathy in a patient with a long-standing history of type 2 diabetes mellitus. Because of the family history of painful sensory neuropathy, we screened for gene variants in those genes encoding Na_Vs that have previously been linked to painful sensory neuropathy: *SCN9*A, *SCN10*A, and *SCN11*A.

Molecular Genetics and Structural Modeling

Generally, our interest is the discovery of rare variants (<1%) as we are looking for variants that potentially have a high impact on channel function, recognizing that not every rare variant will have a large effect, and that there is a small number of relatively common variants that confer gain-of-function attributes on Na_Vs in the context of painful neuropathy (Waxman et al., 2014).

Sequencing of *SCN9A* and *SCN11A* genes, encoding for the $Na_V1.7$ and $Na_V1.9$s, respectively, did not identify any pathogenic variants; there were no rare variants (<1%) in these channels or variants that had previously been linked to painful neuropathy. However, a potentially pathogenic variant (c.724T>A, rs140288103) was found in *SCN10A*, the gene that encodes $Na_V1.8$. The c.724T>A missense variant changes the amino acid 242 of $Na_V1.8$ channel from a serine to a threonine (S242T). The variant was present at a low frequency (MAF 0.0002) in both the Exome Variant Database and Exome Aggregation Consortium databases. Prediction programs Align GVGD, SIFT, and PolyPhen-2 classified the substitution S242T as "C55, likely to interfere with function," "deleterious," and "probably damaging," respectively. S242 is located in the domain (D) I S4-S5 linker of $Na_V1.8$ and is invariant in the Na_V family (Fig. 1A). A homologous mutation S241T in $Na_V1.7$ has been reported previously in families with the pain disorder IEM in Europe (Michiels et al., 2005) and North America (Geha et al., 2016).

We implemented structural modeling based on the recently reported structure of the eukaryotic sodium channel from electric eel (Yan et al., 2017) using the MOE program. The homology modeling was performed using MOE defaults. Since the eel structure published by Yan et al. (2017) did not resolve the intracellular loops L1 (between DI and DII) and L2 (between DII and DIII), the corresponding amino acid sequences of $hNa_V1.7$ and $hNa_V1.8$ were removed before performing the homology modeling (Fig. 1B). Our homology model shows that the location of the S242T residue within the DI/S4-S5 linker and the orientation of the side chain matches exactly the $Na_V1.7$-S241T residue (Fig. 1B), which

Downloaded from molpharm.aspetjournals.org at ASPET Journals on January 13, 2020

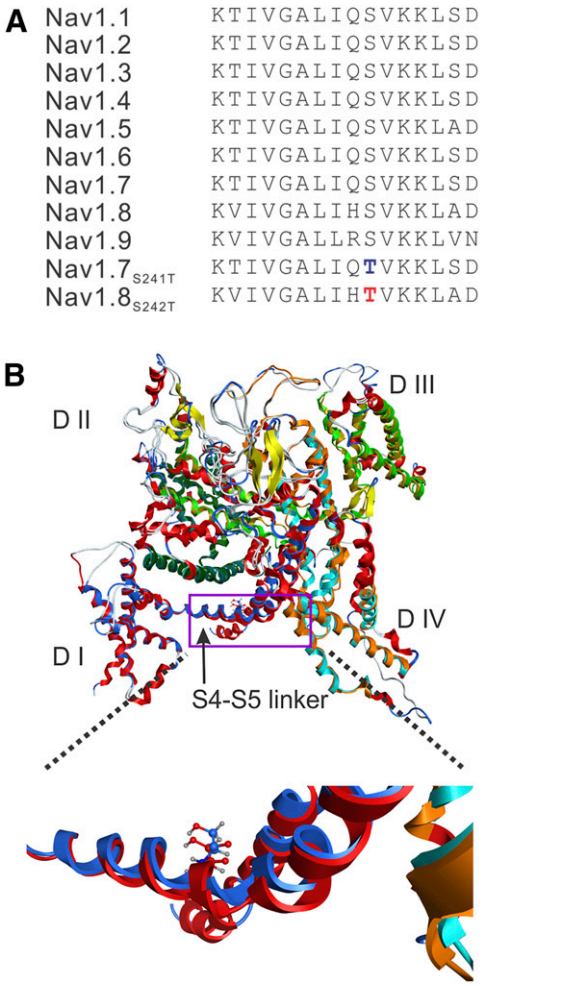

Fig. 1. (A) Sequence alignment and position of mutation in the DI S4-S5 linker in the $Na_V1.8$ channel. The sequence of the DI S4-S5 linker is invariant in the nine sodium channels from humans. The substitution of S242T is highlighted in red type, and the substitution of $Na_V1.7$-S241T is highlighted in blue type. (B) Structural modeling of human $Na_V1.8$ and human $Na_V1.7$ channels. The two channel structures were superimposed, and the membrane-spanning segments showed good alignment. DI is colored blue in $Na_V1.8$, and red in $Na_V1.7$. The overall structure is tilted and rotated to give a clearer view of the DI S4-S5 linker where the S242T and $Na_V1.7$-S241T substitution occurs. A box is drawn to indicate the region of the structure that is zoomed out to better show the $Na_V1.8$-T242 residue (blue carbons) and $Na_V1.7$-T241 residue (red carbons). The serine-to-threonine substitution in the DI S4-S5 linker in $Na_V1.7$ and $Na_V1.8$ maintains the same position and orientation of the side chain.

suggests that the serine-to-threonine substitution in this linker confers similar physiologic and pharmacological attributes on $Na_V1.8$ as it does on $Na_V1.7$.

Functional Analysis of S242T Mutant Channels

Voltage-Clamp Analysis. Voltage-clamp recordings were obtained from DRG neurons from $Na_V1.8$-null mice transfected with WT or S242T mutant channels. Figure 2A shows representative human $Na_V1.8$ sodium currents recorded from cells expressing WT channels, and Fig. 2B shows cells expressing S242T mutant channels. The current density in cells expressing S242T channels was not different from that of WT channels (WT: 325 ± 49 pA/pF, $n = 26$; S242T: 267 ± 30 pA/pF, $n = 30$; $P = 0.315$, t test). The midpoint of activation for S242T ($V_{1/2}$) was shifted by −6.1 mV to −17.82 ± 1.35 mV [95% confidence interval (CI): −20.58 to −15.05 mV; $n = 30$], compared with WT channels (−11.73 ± 0.97 mV; 95% CI: −13.74 to −9.73 mV; $n = 26$; $P = 0.0006$; t test) (Fig. 2C). The kinetics of activation were investigated by measuring the time-to-peak of the transient current. Considering the observed shift in $V_{1/2}$ of activation induced by the S242T mutation, we expected faster activation depending on the step voltage. Activation of S242T channels from −40 to −10 mV was statistically significantly (two-tailed t test with Bonferroni correction, $^*P < 0.05$) faster than that of WT channels (Fig. 2D). We also measured the kinetics of deactivation. As shown in Fig. 2E, the rates of current decay of S242T mutant channels were statistically significantly (two-tailed t test with Bonferroni correction, $^*P < 0.05$) slower than those of WT channels at deactivation potentials from −30 to −10 mV.

The $V_{1/2}$ of fast inactivation for S242T channels (−38.24 ± 1.08 mV, $n = 25$) was hyperpolarized by 3.8 mV compared with that for WT channels (−34.47 ± 0.86 mV, $n = 24$, $P = 0.0088$, t test) (Fig. 2F). As Fig. 2G shows, steady-state slow inactivation of S242T channels was enhanced, compared with WT channels. The $V_{1/2}$ of S242T channels (−56.11 ± 1.21 mV, $n = 13$) was hyperpolarized by 8.9 mV compared with that of WT channels ($V_{1/2}$: −47.20 ± 1.56 mV, $n = 14$; $P = 0.0001$, two-tailed t test).

We measured the response of WT and S242T channels to a slow ramp stimulus. The ramp current for S242T channels (22.60% ± 1.45% of peak current, $n = 26$) was not different from that of WT channels (22.54% ± 0.92% of peak current, $n = 25$; $P = 0.974$, two-tailed t test); however, the average voltage where the peak of ramp current occurs was shifted by −6.4 mV for S242T channels (−22.77 ± 1.44 mV, $n = 26$) compared with that for WT channels (−16.34 ± 0.80 mV, $n = 25$; $P = 0.0004$, two-tailed t test) (Fig. 2H). Figure 2I compares the normalized amplitudes of persistent currents in DRG neurons expressing WT and S242T channels. The persistent currents of S242T channels were statistically significantly (two-tailed t test with Bonferroni correction, $^*P < 0.05$) larger than the persistent currents of WT channels over the voltage from −50 to −25 mV, whereas the S242T mutant channels produced smaller persistent currents than WT channels at more depolarized voltages between −10 and +20 mV.

Current-Clamp Analysis. We assessed the effect of the S242T mutant channels at the cellular level using current-clamp recordings on DRG neurons from $Na_V1.8$-null mice transfected with either WT or S242T channels. The resting membrane potential of DRG neurons expressing S242T channels (−55.6 ± 1.4 mV, $n = 29$) was comparable to that of DRG neurons expressing WT channels (−54.9 ± 1.1 mV, $n = 31$; $P = 0.728$, t test). The input resistance of DRG neurons expressing S242T channels (362 ± 32 MΩ, $n = 29$) was also comparable to that of DRG neurons expressing WT channels (319 ± 38 MΩ, $n = 31$; $P = 0.391$, t test).

Current threshold, the minimal stimulus required to produce a single all-or-none action potential, was reduced in DRG neurons expressing S242T mutant channels. Figure 3A shows traces from a representative DRG neuron expressing WT channels. In response to ≤105 pA subthreshold current injections, the neuron only generated small, graded membrane potential depolarization. The first all-or-none action potential required a stimulus of 110 pA (current threshold for this neuron). Figure 3B shows recordings from a

Downloaded from molpharm.aspetjournals.org at ASPET Journals on January 13, 2020

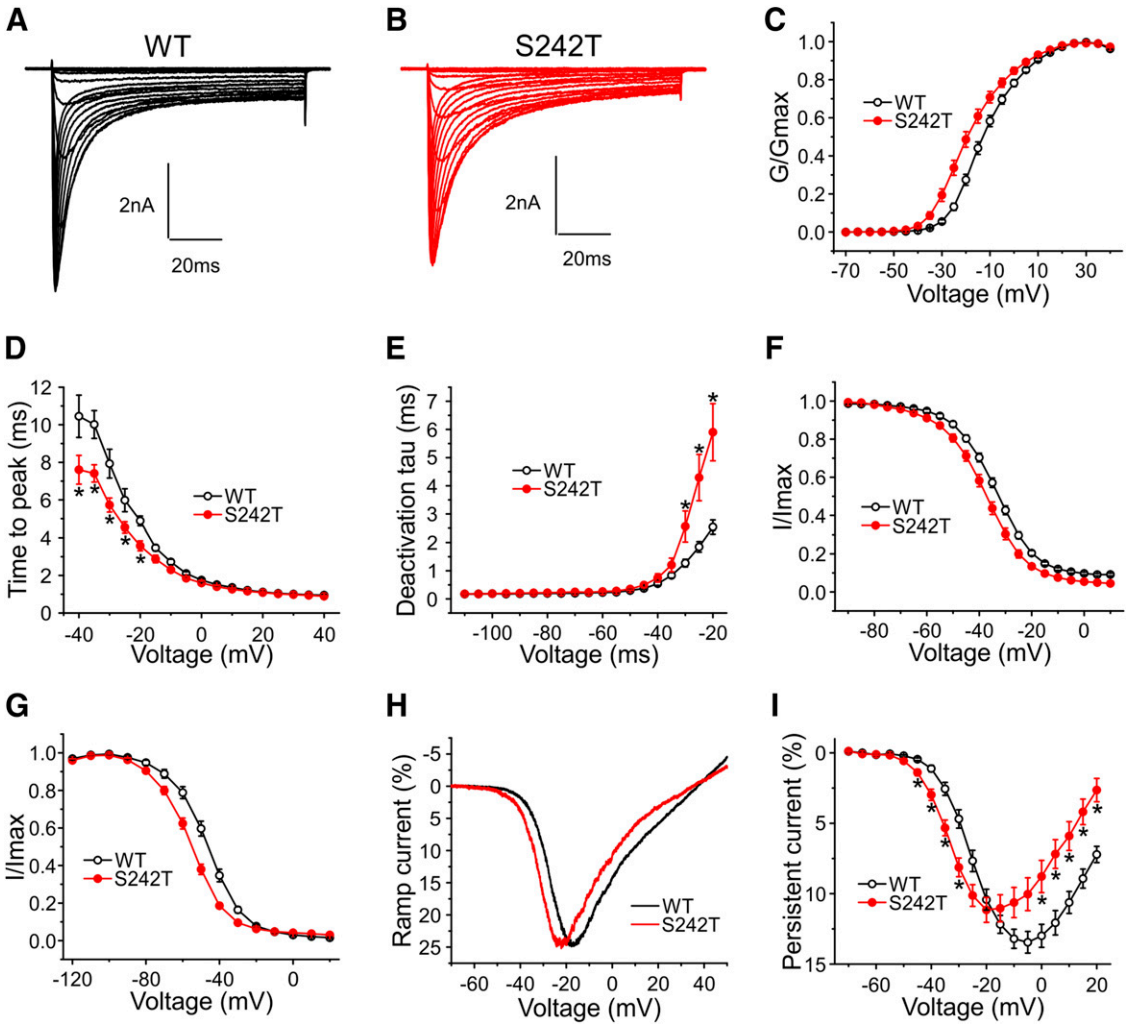

Fig. 2. Voltage-clamp analysis of $Na_V1.8$/S242T mutant channels. Representative current traces recorded from $Na_V1.8$-null DRG neurons expressing WT (A) or S242T (B) channels. (C) Point-to-point curve of the mean G value of WT and S242T channels, which shows that the $V_{1/2,act}$ of S242T ($n = 30$) channels is hyperpolarized by 6.1 mV compared with WT ($n = 26$) channels (two-tailed t test, $P = 0.0006$). (D) Point-to-point curve for mean time-to-peak shows that mutant S242T channels ($n = 29$) opens faster than WT ($n = 25$) at voltages from −40 to −10 mV (two-tailed t test with Bonferroni correction, $^*P < 0.05$). (E) S242T ($n = 24$) channels deactivate significantly slower than WT ($n = 21$) channels at voltages from −30 to −20 mV (two-tailed t test with Bonferroni correction, $^*P < 0.05$). (F) Compared with WT ($n = 24$), the S242T mutation ($n = 25$) shifts $V_{1/2}$ for fast inactivation by −3.8 mV in a hyperpolarized direction. (G) Compared with WT ($n = 14$), the S242T mutation ($n = 13$) enhances steady-state slow-inactivation with the $V_{1/2}$ shifting by −8.9 mV. (H) Representative ramp currents for WT and S242T mutant. Compared with WT ($n = 25$) channels, S242T ($n = 16$) shifts the voltage at which the peak of ramp current occurs. (I) Comparison of persistent currents between cells expressing WT ($n = 26$) channels and cells expressing S242T ($n = 30$) mutant channels for activation depolarization step pulses from −70 to 20 mV. Two-tailed t test with Bonferroni correction, $^*P < 0.05$.

representative DRG neuron that expressed S242T mutant channels. For this neuron, the current injection required to produce the first all-or-none action was 70 pA. Figure 3C presents a comparison of current threshold for a population of these two groups of neurons. The average threshold for DRG neurons expressing S242T mutant channels (64 ± 14 pA, n = 29; 95% CI: 34–93 pA) was smaller compared with that of neurons expressing WT channels (124 ± 21 pA, n = 31; 95% CI: 81–166 pA; P = 0.0079, Mann-Whitney test). There was no difference for action potential amplitude (WT: 110.4 ± 1.6 mV, n = 31; S242T: 111.4 ± 1.9 mV, n = 29; P = 0.700, t test) or the half-width of the action potential (WT: 8.28 ± 0.73 milliseconds, n = 31; S242T: 8.01 ± 0.58 milliseconds, n = 29; P = 0.770, t test) between the two groups of DRG neurons.

The effect of WT and S242T channels on the repetitive firing properties of DRG neurons was assessed by applying a series of 500-millisecond current injections to the two groups of DRG neurons. Representative action potentials triggered by increasing current injections of 150, 300, and 450 pA in neurons transfected with either WT or S242T channels are illustrated in Fig. 3, D–I. Cells expressing S242T (Fig. 3, G–I) fired with a higher frequency than cells expressing WT channels (Fig. 3, D–F) in response to similar stimuli. The average numbers of action potentials in cells expressing WT or S242T elicited by graded current injections in 50-pA steps are plotted in Fig. 3J. Compared with neurons expressing WT channels, neurons expressing S242T channels produced higher firing frequencies at every stimulus level across the broad range studied, which reached statistical significance (two-way ANOVA, genotype × stimulus strength, $P < 0.001$). In addition, we observed that among both groups of DRG neurons, a subpopulation of neurons fired spontaneously. The proportion of spontaneously firing neurons for the group of DRG neurons expressing S242T channels (23 of 52 cells, 44.2%) was not different from that of

Downloaded from molpharm.aspetjournals.org at ASPET Journals on January 13, 2020

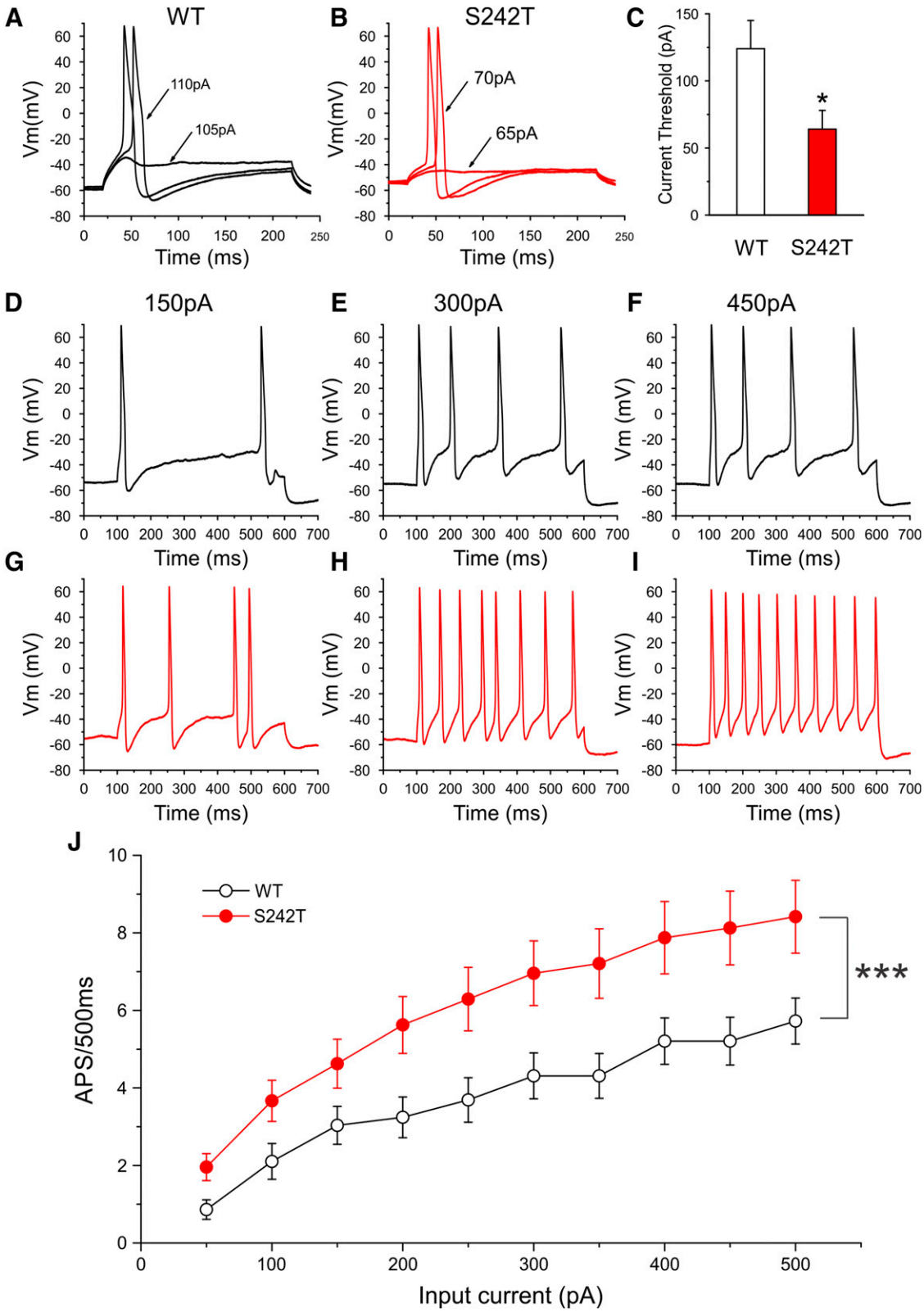

Fig. 3. Current-clamp analysis of effects of S242T mutant channels on DRG neuron excitability. (A and B) Representative action potential (AP) traces recorded from DRG neuron expressing WT (A) or S242T mutant (B) channels. Action potentials were elicited by 200-millisecond step depolarizing current injections from resting membrane potential (V_m). (C) Comparison of current threshold for DRG neurons expressing WT (n = 31) and S242T (n = 29) mutant channels. Expression of S242T channels reduces the current threshold significantly. Two-tailed t test, $^*P < 0.05$. Responses of a representative DRG neuron expressing WT channels (D–F) or S242T mutant channels (G–I) to 500-millisecond depolarization current steps that are 150 pA (left), 300 pA (middle), and 450 pA (right). (J) Comparison of responses (number of impulses evoked by a 500-millisecond stimulus) for the populations of DRG neurons expressing WT (n = 29) or S242T (n = 24) channels across a range of step current injections from 50 to 500 pA. Two-way ANOVA, $^{***}P < 0.001$.

Downloaded from molpharm.aspetjournals.org at ASPET Journals on January 13, 2020

DRG neurons expressing WT channels (15 of 46 cells, 32.6%; $P = 0.235$, two-portion z test).

We would note that our recordings were made in DRG neurons transfected with WT or mutant $Na_V1.8$ channels, and thus express these channels at higher than normal levels, which is why, as in our prior studies (Faber et al., 2012a,b; Huang et al., 2013; Han et al., 2014, 2015), we performed a head-to-head comparison of the effects of the expression of these channels in these neurons. We consider the difference in the neuronal behavior as the indicator of increased excitability induced by mutant channels.

Responsiveness of S242T Mutant Channels to CBZ

CBZ Rescues the Hyperpolarizing Shift of Activation of S242T Mutant Channels. We have previously shown that the pretreatment of cells with a clinically achievable concentration of CBZ (30 μM) (Breton et al., 2005) for 30 minutes depolarizes the voltage dependence of the activation of $Na_V1.7$ channels that carry the S241T substitution (Yang et al., 2012) at the analogous position to the S242T in $Na_V1.8$ (Fig. 1A). Since the homology structure model shows that the spatial location of the S242T residue corresponds with that of the $Na_V1.7$-S241T residue (Fig. 1B), we hypothesized that S242T might also be CBZ responsive. To test this hypothesis, DRG neurons expressing S242T mutant channels were pretreated with DMSO or 30 μM CBZ for 30 minutes before the recordings. Figure 4, A and B, shows representative traces recorded from DRG neurons expressing S242T mutant channels after treatment with DMSO or CBZ, respectively. As Fig. 4C shows, CBZ treatment caused a depolarizing shift of 6.8 mV in the $V_{1/2}$ of voltage dependence of activation of S242T mutant channels compared with DMSO treatment (DMSO: -18.00 ± 2.14 mV, $n = 12$; 95% CI: -22.72 to -13.29 mV; CBZ: -11.19 ± 1.80 mV, $n = 17$; 95% CI: -15.00 to -7.39 mV; $P = 0.023$, t test). The treatment of DRG neurons with 30 μM CBZ did not shift steady-state fast inactivation of S242T mutant channels (Fig. 4D). The $V_{1/2}$ of steady-state fast inactivation for CBZ treatment (-38.20 ± 2.93 mV, $n = 11$) was not different from that for DMSO treatment (-37.54 ± 2.86 mV, $n = 7$; $P = 0.875$, t test). Treatment with 30 μM CBZ also did not cause a statistically significant shift in the steady-state slow inactivation of S242T mutant channels. The $V_{1/2}$ of steady-state slow inactivation after DMSO treatment and CBZ treatment were -50.84 ± 1.59 mV ($n = 13$) and -56.14 ± 3.11 mV ($n = 11$; $P = 0.150$, t test), respectively.

CBZ Does Not Shift Activation of WT Channels. To determine whether CBZ treatment shifts the activation of $Na_V1.8$-WT channels, we incubated DRG neurons expressing WT channels with 30 μM CBZ or DMSO. Figure 5, A and B, shows representative traces recorded from DRG neurons expressing WT channels after being treated with DMSO or CBZ, respectively. CBZ treatment did not shift the voltage dependence of activation of WT channels ($V_{1/2,act}$: DMSO, -13.49 ± 2.13 mV, $n = 10$; CBZ, -11.44 ± 1.64 mV, $n = 14$; $P = 0.454$, two-tailed t test) (Fig. 5C). Treatment with 30 μM CBZ did not shift the steady-state fast inactivation of WT channels (Fig. 5D) ($V_{1/2}$ of fast-inactivation: DMSO, -36.26 ± 2.36 mV, $n = 10$; CBZ, -36.84 ± 2.05 mV, $n = 14$; $P = 0.855$, t test), or steady-state slow-inactivation ($V_{1/2}$ of steady-state slow inactivation: DMSO, -46.04 ± 2.12 mV, $n = 13$; CBZ, -46.74 ± 1.56 mV, $n = 13$; $P = 0.793$, two-tailed t test).

CBZ Reduces Excitability of DRG Neurons Expressing S242T Mutant Channels. As shown above, the expression of S242T mutant channels increased the excitability of DRG neurons. Because pretreatment with CBZ depolarized the activation of S242T mutant channels, shifting their $V_{1/2,act}$ value to a voltage close to that of WT channels (Fig. 4C), we hypothesized that pretreatment with CBZ should attenuate the

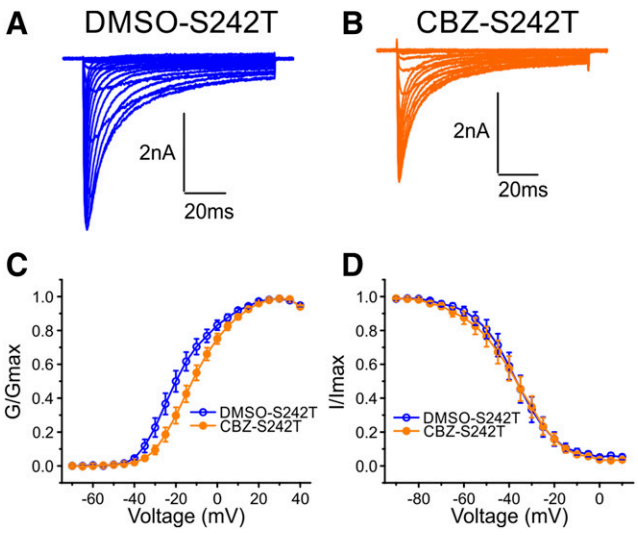

Fig. 4. Clinically relevant concentration of CBZ rescued the hyperpolarizing shift of activation of S242T mutant channels. Representative traces of current families recorded from DRG neurons expressing S242T mutant channel treated with DMSO (A) or with 30 μM CBZ (B). (C) Treatment with CBZ ($n = 17$) significantly shifted the voltage-dependence of activation of the S242T mutant channel compared with the treatment with DMSO ($n = 12$); two-tailed t test. (D) Treatment with 30 μM CBZ ($n = 11$) did not affect the voltage dependence of steady-state fast inactivation compared with the treatment with DMSO ($n = 7$).

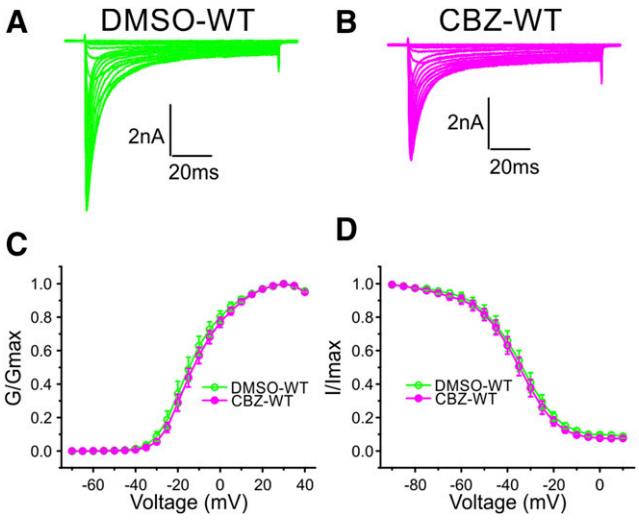

Fig. 5. A clinically relevant concentration of CBZ had no effect on WT channels. Representative traces of current families recorded from DRG neurons expressing WT channels treated with DMSO (A) or with 30 μM CBZ (B). (C) Treatment with CBZ ($n = 14$) did not shift the voltage-dependence of activation of WT channels compared with treatment with DMSO ($n = 10$). (D) Treatment with 30 μM CBZ ($n = 14$) did not affect the voltage-dependence of steady-state fast inactivation compared with the treatment with DMSO ($n = 10$).

Downloaded from molpharm.aspetjournals.org at ASPET Journals on January 13, 2020

increased excitability of DRG neurons expressing S242T mutant channels. Current-clamp recording was implemented to evaluate the effect of CBZ pretreatment on the excitability of DRG neurons expressing S242T mutant channels.

Pretreatment of transfected DRG neurons with 30 μM CBZ for 30 minutes did not alter the resting membrane potential of DRG neurons expressing S242T channels compared with the DMSO control (DMSO: -52.0 ± 1.1 mV, $n = 28$; CBZ: -54.5 ± 0.8 mV, $n = 29$; $P = 0.078$, two-tailed t test). The input resistance of DRG neurons expressing S242T channels was not different between cells treated with CBZ (315 ± 55 MΩ, $n = 29$) or DMSO (366 ± 62 MΩ, $n = 28$; $P = 0.545$, two-tailed t test). Figure 6A shows traces of a representative neuron expressing S242T mutant channels treated with DMSO. The current threshold for this neuron was 55 pA. In contrast, Fig. 6B shows traces of a representative neuron expressing S242T mutant channels treated with CBZ, and the current threshold for this neuron was 90 pA. On average, CBZ treatment doubled the current threshold for DRG neurons expressing S242T mutant channel (DMSO: 55 ± 8 pA, $n = 28$; 95% CI, 39–71 pA; CBZ: 114 ± 21 pA, $n = 29$; $P = 0.012$; 95% CI, 71–157 pA; $P = 0.037$, Mann-Whitney test; Fig. 6C). However, there was no difference in action potential amplitude between the CBZ- and DMSO-treated neurons (DMSO: 104.5 ± 1.8 mV, $n = 28$; CBZ: 106.4 ± 1.5 mV, $n = 29$; $P = 0.417$, t test). The half-width of action potential was also not different between the two groups of DRG neurons (DMSO: 8.33 ± 0.83 mV, $n = 28$; CBZ: 9.78 ± 1.25 mV, $n = 29$; $P = 0.338$, two-tailed t test).

We further investigated the effect of CBZ treatment on the firing frequency of DRG neurons expressing S242T mutant channels. As shown in Fig. 6, D–F, a neuron treated with DMSO produced multiple action potentials in response to 500-millisecond depolarizing current steps of 150, 300, and 450 pA. In contrast, a neuron treated with CBZ (Fig. 6, G–I) generated fewer action potentials in response to the same current injections. Compared with the treatment with DMSO, the treatment with CBZ caused a marked reduction in the firing frequencies for DRG neurons expressing S242T mutant channels, which reached statistical significance (two-way ANOVA, treatment × stimulus strength, $P < 0.001$) (Fig. 6J). Although we observed a reduction in the proportion of spontaneously firing neurons treated with CBZ (DMSO: 45.1%; 23 of 51 cells; CBZ: 35.1%; 16 of 45 cells), this difference did not reach statistical significance ($P = 0.315$, two-portion z-test). These data show that CBZ treatment attenuated the hyperexcitability of DRG neurons expressing S242T mutant channels.

CBZ Does Not Cause Reduction in the Excitability of DRG Neurons Expressing WT Channels. We evaluated whether treatment with 30 μM CBZ for 30 minutes attenuates the excitability of DRG neurons expressing WT channels. Figure 7, A and B, shows traces of two representative neurons expressing WT channels after treatment with DMSO or 30 μM CBZ, respectively. Current threshold for these two neurons were 155 pA (DMSO) (Fig. 7A) and 135 pA (CBZ) (Fig. 7B). On average, the current threshold for DRG neurons expressing WT channels after treatment with CBZ (137 ± 23 pA, $n = 27$) was not different from that of neurons treated with DMSO (132 ± 24 pA, $n = 25$; $P = 0.912$, Mann-Whitney test) (Fig. 7C). We also found that treatment with CBZ had no effects on resting membrane potential (DMSO: -54.8 ± 1.4 mV, $n = 25$; CBZ: -55.1 ± 1.3 mV, $n = 27$; $P = 0.875$, t test), input resistance (DMSO: 313 ± 43 MΩ, $n = 25$; CBZ: 264 ± 41 MΩ, $n = 27$), amplitude (DMSO: 105.7 ± 1.5 mV, $n = 25$; CBZ: 107.8 ± 1.2 mV, $n = 27$; $P = 0.277$, t test), and half-width (DMSO: 9.51 ± 1.07 milliseconds, $n = 25$; CBZ: 9.55 ± 1.11 milliseconds, $n = 27$; $P = 0.977$, t test) of action potentials.

We compared the firing frequency of DRG neurons expressing WT channels after treatment with CBZ or DMSO. Figure 7, D–I, shows responses of two representative DRG neurons expressing WT channels after treatment with DMSO (Fig. 7, D–F) or CBZ (Fig. 7, G–I). Both neurons produced the same or nearly the same number of spikes in response to 150-, 300-, or 450-pA current injection. As summarized in Fig. 7J, across the range of current stimuli we studied, treatment with CBZ resulted in a small but statistically significant difference in the firing frequency of DRG neurons expressing WT channels compared with treatment with DMSO (two-way ANOVA, treatment × stimulus strength, $P < 0.05$). In addition, compared with DMSO treatment, CBZ treatment did not change the proportion of spontaneously firing neurons (DMSO: 13 of 38 cells, 34.2%; CBZ: 11 of 38 cells, 28.9%; $P = 0.619$, two-portion z-test).

Discussion

We report here the novel S242T mutation in a patient with neuropathic pain and DPN. Voltage-clamp recordings in DRG neurons show that S242T confers a complex phenotype at the channel level, manifesting both gain-of-function attributes, including a hyperpolarizing shift of activation, and loss-of-function attributes, including a hyperpolarizing shift in slow inactivation. Current-clamp recordings demonstrated that S242T mutant channels render DRG neurons hyperexcitable, indicating a dominant role for the gain-of-function attributes, consistent with neuropathic pain in this patient. We previously showed (Yang et al., 2012) that the homologous S241T mutation in $Na_V1.7$ endows this channel with a unique mode of responsiveness to CBZ: depolarization of voltage dependence of activation. We demonstrate here that CBZ depolarizes the voltage dependence of activation of the S242T mutant channel and reduces the excitability of DRG neurons expressing these channels. These data suggest that the novel activity of CBZ as an activation modulator extends from $Na_V1.7$ to $Na_V1.8$.

The presence of this mutation could not be assessed in the deceased father, preventing analysis of genetic segregation. Nevertheless, our data suggest that S242T might be "pathogenic" or "probably pathogenic" based on criteria that have been established for the analysis of variants in Na_Vs (Waxman et al., 2014). The variant was absent in the cohort of patients with diabetes who did not have pain and is exceedingly rare in the genomic databases (MAF 0.0002). In silico analysis identified S242T as damaging and deleterious. The S242T mutation occurs at a position in the DI/S4-5 linker where there is a homologous gain-of-function mutation in $Na_V1.7$ that causes IEM (Michiels et al., 2005; Lampert et al., 2006; Geha et al., 2016). As shown in this study, functional assessment of S242T shows that it confers gain-of-function attributes on $Na_V1.8$ and renders DRG neurons hyperexcitable. One possible explanation for the late onset of symptoms is that an altered metabolic milieu secondary to diabetes, for example elevated methylglyoxal, which has been shown previously to depolarize $Na_V1.8$ inactivation (Bierhaus et al., 2012), further

Downloaded from molpharm.aspetjournals.org at ASPET Journals on January 13, 2020

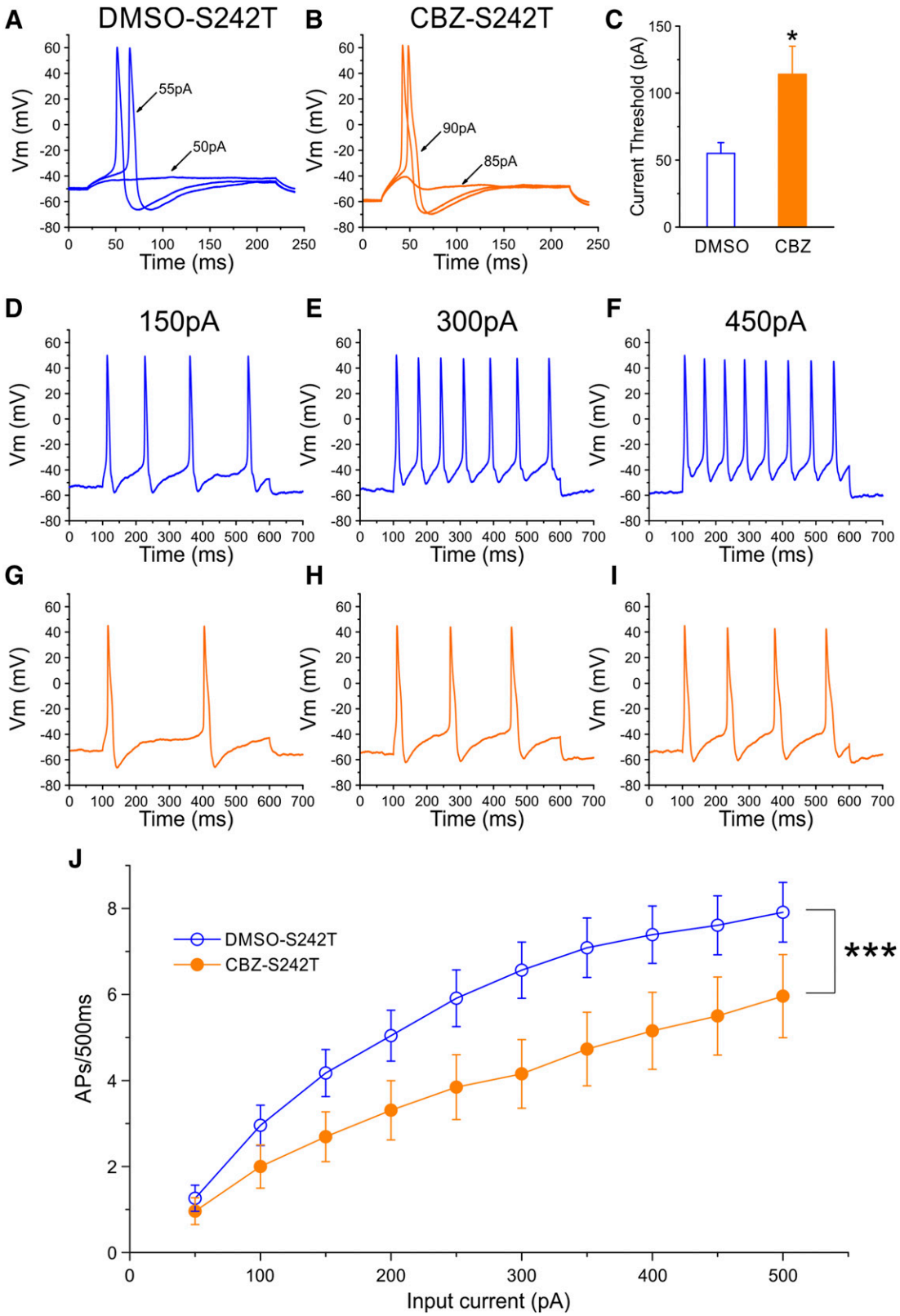

Fig. 6. Current-clamp analysis of the effects of CBZ treatment on DRG neurons expressing S242T mutant channels. Representative action potential (AP) traces recorded from DRG neuron expressing S242T mutant channels after treatment with DMSO (A) or 30 μM CBZ (B). (C) Comparison of current threshold for DRG neurons expressing S242T mutant channels after treatment with CBZ (n = 29) or DMSO (n = 28) control. CBZ treatment increased current threshold significantly. Two-tailed t test, $^*P < 0.05$. Responses of a representative DRG neurons expressing S242T mutant channels after the treatment with DMSO (D–F) or CBZ (G–I) to 500-millisecond depolarization current steps of 150 pA (left), 300 pA (middle), and 450 pA (right). (J) Comparison of responses (number of impulses evoked by a 500-millisecond stimulus) in the population of DRG neurons expressing S242T mutant channels with treatment with CBZ (n = 26) or DMSO (n = 23) control across a range of step current injections from 50 to 500 pA. Two-way ANOVA, $^{***}P < 0.001$. V_m, membrane potential.

Downloaded from molpharm.aspetjournals.org at ASPET Journals on January 13, 2020

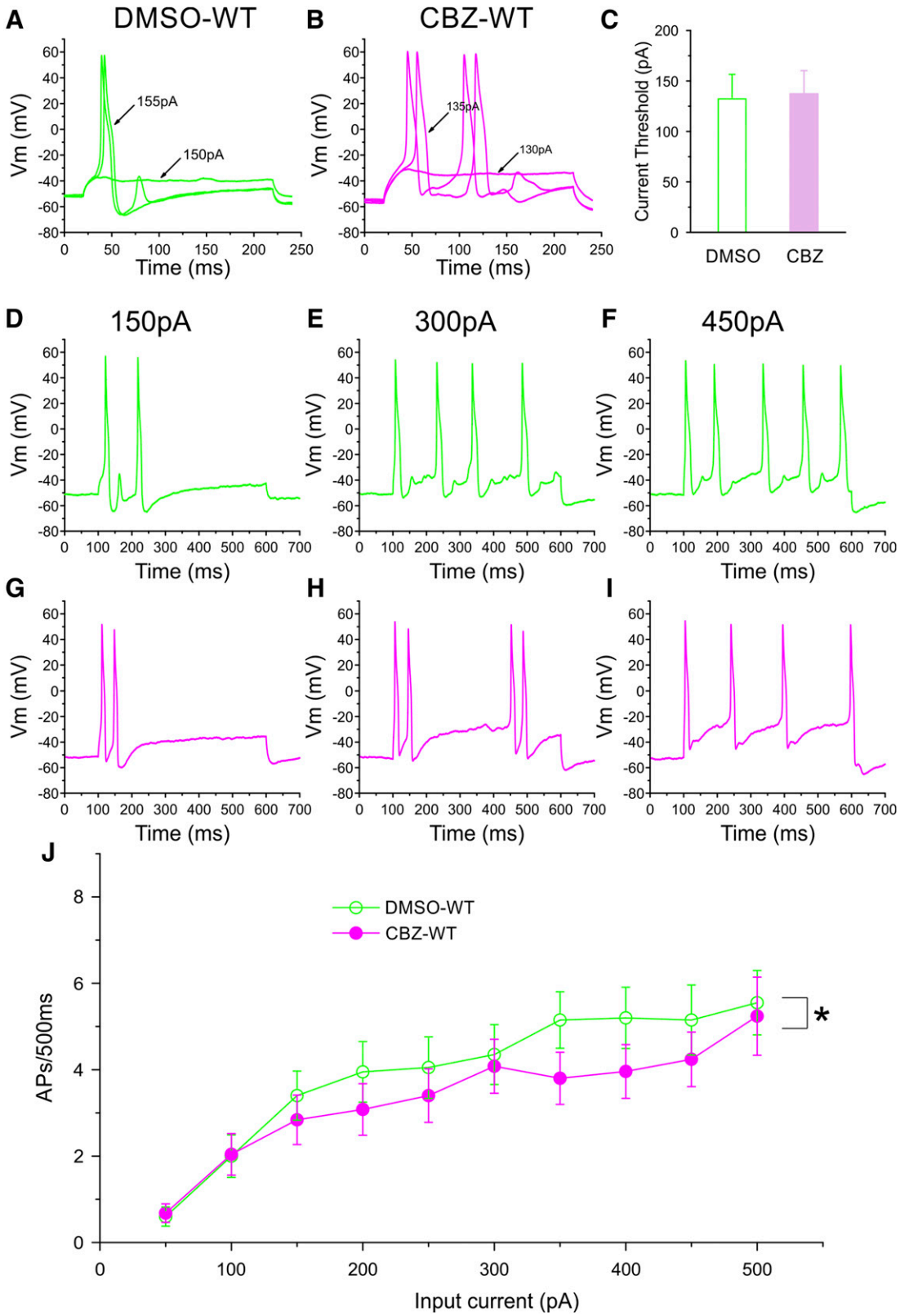

Fig. 7. Current-clamp analysis of the effects of CBZ treatment on DRG neurons expressing WT channels. Representative action potential (AP) traces recorded from DRG neurons expressing WT channels after treatment with DMSO (A) or 30 μM CBZ (B). (C) Comparison of current threshold for DRG neurons expressing WT channels after treatment of CBZ (n = 27) or DMSO (n = 25) control. CBZ treatment did not have a significant effect on current threshold. Responses of the representative DRG neurons expressing WT channels after treatment with DMSO (D–F) or CBZ (G–I) to 500-millisecond depolarization current steps of 150 pA (left), 300 pA (middle), and 450 pA (right). (J) Comparison of responses (number of impulses evoked by a 500-millisecond stimulus) in the population of DRG neurons expressing WT channels with treatment with CBZ (n = 25) or DMSO (n = 20) control across a range of step current injections from 50 to 500 pA. Two-way ANOVA, $^*P < 0.05$. V_m, membrane potential.

Downloaded from molpharm.aspetjournals.org at ASPET Journals on January 13, 2020

enhancing the gain-of-function attributes of the mutant channel, may have been required for the full manifestation of clinical symptoms. However, this is a small study with genetic and clinical data available for only one patient, and, given the fact that DPN is potentially a gene-environment interaction, large cohorts will be needed for replication and to establish pathogenicity.

The S242T substitution within the DI/S4-S5 linker is homologous to the $Na_V1.7$-S241T mutation, which has been identified in subjects with IEM (Michiels et al., 2005; Geha et al., 2016). Homology modeling based on the cryogenic electron microscopy structure of the electric eel sodium channel (Yan et al., 2017) shows a conserved position and orientation of the S/T substitution in $Na_V1.7$ and $Na_V1.8$. The S4-5 linker transduces the movement of the voltage sensor into a conformational change in the pore module during opening of the activation gate (Payandeh et al., 2011), which suggests that the activation properties of the $Na_V1.8$ mutant channel would be altered by this substitution. Indeed, voltage-clamp recordings showed that, similar to the effect of the S241T substitution on $Na_V1.7$, S242T channel activation is hyperpolarized and accelerated, and deactivation is slowed, all of which are gain-of-function features. However, unlike the $Na_V1.7$-S241T channels, S242T channels displayed enhanced fast and slow inactivation, both of which are loss-of-function features. Enhanced fast inactivation has not been previously reported for mutations of the S4-5 linkers in $Na_V1.7$-S241T or $Na_V1.7$-I234T; however, the $Na_V1.7$-I234T mutation in the S4-5 linker manifests massive enhancement of slow inactivation by about −20 mV (Ahn et al., 2010). Local structural alterations due to intramolecular interactions of the S/T substitution or altered interactions of the threonine mutant residue with phospholipids in the plasma membrane might produce channel isoform-specific effects on gating.

Because the S242T mutation confers both gain-of-function (hyperpolarized and accelerated activation and slower deactivation) and loss-of-function (enhanced fast and slow inactivation) biophysical attributes on $Na_V1.8$, it was not possible to predict a priori whether it would increase neuronal excitability. Current-clamp analysis showed that the S242T channels rendered DRG neurons hyperexcitable, which was manifested as reduced current threshold and increased evoked firing. It is well established that DRG neurons sit at resting potentials in the −50 to −60 mV range (Fang et al., 2006; Faber et al., 2012a,b; Hendrich et al., 2012), and a hyperpolarizing shift in activation of $Na_V1.8$ and an increase in persistent current close to the resting potential of these neurons would be expected to increase excitability (Huang et al., 2018). Hyperpolarized and accelerated activation and increased persistent currents at relatively hyperpolarized potentials of S242T compared with WT channels would be expected to increase the excitability of DRG neurons. The increased excitability of DRG neurons that we observed (Fig. 4) is consistent with the pain reported by the patient carrying the S242T mutation.

Building upon the observation that CBZ depolarizes the voltage dependence of the activation of $Na_V1.7$-S241T channels (Yang et al., 2012) and attenuates the excitability of DRG neurons expressing these channels (Geha et al., 2016), we reasoned that the S242T mutation in $Na_V1.8$, which corresponds to S241T in $Na_V1.7$, would be CBZ responsive. Our data show that the clinically achievable concentration of CBZ (30 μM) also depolarizes the voltage dependence of the activation of S242T channels (Fig. 4C) and attenuates the firing of DRG neurons expressing the mutant channel (Fig. 6). By contrast, similar treatment with CBZ of DRG neurons expressing WT $Na_V1.8$ channels did not depolarize the voltage dependence of activation of the channel (Fig. 5) and only slightly reduced the firing of DRG neurons (Fig. 7). Although a CBZ concentration of 30 μM could act on other sodium channels, our data suggest that the attenuation of firing of neurons expressing the mutant channel is more likely due to the effect of CBZ as an activation modifier. This conclusion is supported by the observation that CBZ pretreatment of DRG neurons that expressed the $Na_V1.7$-F1449V mutant channels, whose activation is not modified by CBZ, did not attenuate the firing of these neurons (Yang et al., 2012).

The normalizing effect of CBZ on the activation of $Na_V1.7$ mutant channels I234T, S241T, and V400M (Fischer et al., 2009; Yang et al., 2012, 2018; Geha et al., 2016) is novel, and has not been previously reported for drugs that bind at the Na_V local anesthetic binding site. This effect is also distinct from classic state-dependent blocking of Na_V channels in that it requires pretreatment with CBZ (Fischer et al., 2009; Yang et al., 2012, 2018; Geha et al., 2016). Whether this novel mode of action of CBZ on $Na_V1.7$ and $Na_V1.8$ mutations is due to the formation of a new binding site is not known. The fact that DI/S4-5 S/T substitution in both channels responded to CBZ in the same manner, however, suggests a common mechanism, despite differences in the primary sequence of the two channels even within the highly conserved linker sequence (Fig. 1A). Elucidation of the molecular determinants of productive drug-target interactions in channels other than $Na_V1.7$ might be useful in establishing molecular and structural requirements for this novel mode of action of CBZ.

A recent systematic review (Finnerup et al., 2015) found that the evidence for efficacy of CBZ in neuropathic pain treatment was inconclusive and noted dose-limiting side effects. CBZ is not therefore used as a first-line treatment of neuropathic pain (first-line treatments include gabapentinoids, tricyclic antidepressants, and serotonin-noradrenaline reuptake inhibitors); however, CBZ is still used clinically in selected patients with some success, especially because of its demonstrable effectiveness in patients with trigeminal neuralgia (Maarbjerg et al., 2017). It is increasingly clear that there are multiple pathophysiological drivers of neuropathic pain, and we need to find better ways of stratifying patients to aid treatment selection (Themistocleous et al., 2018). A recent study (Demant et al., 2014) reported that patients with a specific pattern of sensory dysfunction termed the "irritable nociceptor" (defined by mechanical hypersensitivity and preserved small fiber function on QST) had a better treatment response to oxcarbazepine compared with those without this feature. A further approach to patient stratification is to use molecular genetics. Recently, patients with S241T and I234T were shown to respond to CBZ treatment, which was predicted using an approach that employed atomic-level structure modeling, mutant cycle analysis, and in vitro pharmacological testing (Yang et al., 2012, 2018; Geha et al., 2016). Thus far, it has been unclear whether this precision medicine approach can be extended to mutations in other sodium channels. Although we could not test the efficacy of CBZ in this subject because of the limitations imposed by the approved protocol, our current-clamp recordings demonstrate that 30 μM CBZ

Downloaded from molpharm.aspetjournals.org at ASPET Journals on January 13, 2020

attenuates S242T-induced hyperexcitability of DRG neurons, suggesting that CBZ treatment might be beneficial for individuals carrying this mutation.

In summary, we have described a novel gain-of-function $Na_V1.8$ mutation in a patient with diabetes and neuropathic pain. S242T mutant channels manifest dominant gain-of-function attributes and render DRG neurons hyperexcitable. Exposure to a clinically achievable concentration of CBZ corrects the mutation-induced hyperpolarized shift of voltage dependence of activation and attenuates the hyperexcitability of DRG neurons expressing S242T channels. Our data suggest that the novel mode of action of CBZ can be extended from $Na_V1.7$ to $Na_V1.8$, and more generally suggest that the precision medicine approach capitalizing on this finding might produce beneficial outcomes to individuals carrying CBZ-responsive $Na_V1.8$ mutations.

Acknowledgments

We thank Palak Shah and Dr. Peng Zhao for technical assistance. We also thank Dr. Daria Sizova, Dr. Yang Yang, Dr. Brian Tanaka, Dr. Jianying Huang, and Dr. Malgorzata Mis for valuable comments.

Authorship Contributions

Participated in research design: Bennett, Waxman, S. D. Dib-Hajj.

Conducted experiments: Han, Themistocleous, Estacion, Blesneac, Fratter.

Contributed new reagents or analytic tools: F. B. Dib-Hajj, Macala.

Performed data analysis: Han, Themistocleous, Estacion, Blesneac, Fratter, Bennett, Waxman, S. D. Dib-Hajj.

Wrote or contributed to the writing of the manuscript: Han, Themistocleous, Estacion, Bennett, Waxman, S. D. Dib-Hajj.

References

Ahn HS, Dib-Hajj SD, Cox JJ, Tyrrell L, Elmslie FV, Clarke AA, Drenth JP, Woods CG, and Waxman SG (2010) A new $Na_v1.7$ sodium channel mutation I234T in a child with severe pain. *Eur J Pain* **14**:944–950.

Akopian AN, Sivilotti L, and Wood JN (1996) A tetrodotoxin-resistant voltage-gated sodium channel expressed by sensory neurons. *Nature* **379**:257–262.

Ambrósio AF, Soares-Da-Silva P, Carvalho CM, and Carvalho AP (2002) Mechanisms of action of carbamazepine and its derivatives, oxcarbazepine, BIA 2-093, and BIA 2-024. *Neurochem Res* **27**:121–130.

Bennett DL and Woods CG (2014) Painful and painless channelopathies. *Lancet Neurol* **13**:587–599.

Bierhaus A, Fleming T, Stoyanov S, Leffler A, Babes A, Neacsu C, Sauer SK, Eberhardt M, Schnölzer M, Lasitschka F, et al. (2012) Methylglyoxal modification of $Na_v1.8$ facilitates nociceptive neuron firing and causes hyperalgesia in diabetic neuropathy [published correction appears in *Nat Med* (2012) 18:1445]. *Nat Med* **18**: 926–933.

Blair NT and Bean BP (2002) Roles of tetrodotoxin (TTX)-sensitive Na+ current, TTX-resistant Na+ current, and Ca2+ current in the action potentials of nociceptive sensory neurons. *J Neurosci* **22**:10277–10290.

Bouhassira D, Attal N, Alchaar H, Boureau F, Brochet B, Bruxelle J, Cunin G, Fermanian J, Ginies P, Grun-Overdyking A, et al. (2005) Comparison of pain syndromes associated with nervous or somatic lesions and development of a new neuropathic pain diagnostic questionnaire (DN4). *Pain* **114**:29–36.

Breton H, Cociglio M, Bressolle F, Peyriere H, Blayac JP, and Hillaire-Buys D (2005) Liquid chromatography-electrospray mass spectrometry determination of carbamazepine, oxcarbazepine and eight of their metabolites in human plasma. *J Chromatogr B Analyt Technol Biomed Life Sci* **828**:80–90.

Bril V and Perkins BA (2002) Validation of the Toronto Clinical Scoring System for diabetic polyneuropathy. *Diabetes Care* **25**:2048–2052.

Compston A (2010) Aids to the investigation of peripheral nerve injuries. Medical Research Council: Nerve Injuries Research Committee. His Majesty's Stationery Office: 1942; pp. 48 (iii) and 74 figures and 7 diagrams; with aids to the examination of the peripheral nervous system. By Michael O'Brien for the guarantors of brain. Saunders Elsevier: 2010; pp. [8] 64 and 94 figures. *Brain* **133**:2838–2844.

Cummins TR, Dib-Hajj SD, Black JA, Akopian AN, Wood JN, and Waxman SG (1999) A novel persistent tetrodotoxin-resistant sodium current in SNS-null and wild-type small primary sensory neurons. *J Neurosci* **19**:RC43.

Demant DT, Lund K, Vollert J, Maier C, Segerdahl M, Finnerup NB, Jensen TS, and Sindrup SH (2014) The effect of oxcarbazepine in peripheral neuropathic pain depends on pain phenotype: a randomised, double-blind, placebo-controlled phenotype-stratified study. *Pain* **155**:2263–2273.

Dib-Hajj SD, Black JA, and Waxman SG (2015) NaV1.9: a sodium channel linked to human pain. *Nat Rev Neurosci* **16**:511–519.

Dib-Hajj SD, Cummins TR, Black JA, and Waxman SG (2010) Sodium channels in normal and pathological pain. *Annu Rev Neurosci* **33**:325–347.

Dib-Hajj SD, Geha P, and Waxman SG (2017) Sodium channels in pain disorders: pathophysiology and prospects for treatment. *Pain* **158** (Suppl 1):S97–S107.

Faber CG, Hoeijmakers JG, Ahn HS, Cheng X, Han C, Choi JS, Estacion M, Lauria G, Vanhoutte EK, Gerrits MM, et al. (2012a) Gain of function $Na_v1.7$ mutations in idiopathic small fiber neuropathy. *Ann Neurol* **71**:26–39.

Faber CG, Lauria G, Merkies IS, Cheng X, Han C, Ahn HS, Persson AK, Hoeijmakers JG, Gerrits MM, Pierro T, et al. (2012b) Gain-of-function Nav1.8 mutations in painful neuropathy. *Proc Natl Acad Sci USA* **109**:19444–19449.

Fang X, Djouhri L, McMullan S, Berry C, Waxman SG, Okuse K, and Lawson SN (2006) Intense isolectin-B4 binding in rat dorsal root ganglion neurons distinguishes C-fiber nociceptors with broad action potentials and high Nav1.9 expression. *J Neurosci* **26**:7281–7292.

Fertleman CR, Baker MD, Parker KA, Moffatt S, Elmslie FV, Abrahamsen B, Ostman J, Klugbauer N, Wood JN, Gardiner RM, et al. (2006) SCN9A mutations in paroxysmal extreme pain disorder: allelic variants underlie distinct channel defects and phenotypes. *Neuron* **52**:767–774.

Finnerup NB, Attal N, Haroutounian S, McNicol E, Baron R, Dworkin RH, Gilron I, Haanpää M, Hansson P, Jensen TS, et al. (2015) Pharmacotherapy for neuropathic pain in adults: a systematic review and meta-analysis. *Lancet Neurol* **14**:162–173.

Fischer TZ, Gilmore ES, Estacion M, Eastman E, Taylor S, Melanson M, Dib-Hajj SD, and Waxman SG (2009) A novel Nav1.7 mutation producing carbamazepine-responsive erythromelalgia. *Ann Neurol* **65**:733–741.

Geha P, Yang Y, Estacion M, Schulman BR, Tokuno H, Apkarian AV, Dib-Hajj SD, and Waxman SG (2016) Pharmacotherapy for pain in a family with inherited erythromelalgia guided by genomic analysis and functional profiling. *JAMA Neurol* **73**:659–667.

Han C, Estacion M, Huang J, Vasylyev D, Zhao P, Dib-Hajj SD, and Waxman SG (2015) Human Na(v)1.8: enhanced persistent and ramp currents contribute to distinct firing properties of human DRG neurons. *J Neurophysiol* **113**:3172–3185.

Han C, Vasylyev D, Macala LJ, Gerrits MM, Hoeijmakers JG, Bekelaar KJ, Dib-Hajj SD, Faber CG, Merkies IS, and Waxman SG (2014) The G1662S NaV1.8 mutation in small fibre neuropathy: impaired inactivation underlying DRG neuron hyperexcitability. *J Neurol Neurosurg Psychiatry* **85**:499–505.

Hendrich J, Alvarez P, Joseph EK, Ferrari LF, Chen X, and Levine JD (2012) In vivo and in vitro comparison of female and male nociceptors. *J Pain* **13**:1224–1231.

Hong S, Morrow TJ, Paulson PE, Isom LL, and Wiley JW (2004) Early painful diabetic neuropathy is associated with differential changes in tetrodotoxin-sensitive and -resistant sodium channels in dorsal root ganglion neurons in the rat. *J Biol Chem* **279**:29341–29350.

Huang J, Mis MA, Tanaka B, Adi T, Estacion M, Liu S, Walker S, Dib-Hajj SD, and Waxman SG (2018) Atypical changes in DRG neuron excitability and complex pain phenotype associated with a $Na_v1.7$ mutation that massively hyperpolarizes activation. *Sci Rep* **8**:1811.

Huang J, Yang Y, Zhao P, Gerrits MM, Hoeijmakers JG, Bekelaar K, Merkies IS, Faber CG, Dib-Hajj SD, and Waxman SG (2013) Small-fiber neuropathy Nav1.8 mutation shifts activation to hyperpolarized potentials and increases excitability of dorsal root ganglion neurons. *J Neurosci* **33**:14087–14097.

Kleyweg RP, van der Meché FG, and Schmitz PI (1991) Interobserver agreement in the assessment of muscle strength and functional abilities in Guillain-Barré syndrome. *Muscle Nerve* **14**:1103–1109.

Kuo CC (1998) A common anticonvulsant binding site for phenytoin, carbamazepine, and lamotrigine in neuronal Na+ channels. *Mol Pharmacol* **54**:712–721.

Kuo CC, Chen RS, Lu L, and Chen RC (1997) Carbamazepine inhibition of neuronal Na+ currents: quantitative distinction from phenytoin and possible therapeutic implications. *Mol Pharmacol* **51**:1077–1083.

Lampert A, Dib-Hajj SD, Tyrrell L, and Waxman SG (2006) Size matters: erythromelalgia mutation S241T in Nav1.7 alters channel gating. *J Biol Chem* **281**: 36029–36035.

Lauria G, Hsieh ST, Johansson O, Kennedy WR, Leger JM, Mellgren SI, Nolano M, Merkies IS, Polydefkis M, Smith AG, et al. (2010) European Federation of Neurological Societies/Peripheral Nerve Society Guideline on the use of skin biopsy in the diagnosis of small fiber neuropathy. Report of a joint task force of the European Federation of Neurological Societies and the Peripheral Nerve Society. *Eur J Neurol* **17**(7):903–912, e44–49.

Maarbjerg S, Di Stefano G, Bendtsen L, and Cruccu G (2017) Trigeminal neuralgia - diagnosis and treatment. *Cephalalgia* **37**:648–657.

Maier C, Baron R, Tölle TR, Binder A, Birbaumer N, Birklein F, Gierthmühlen J, Flor H, Geber C, Huge V, et al. (2010) Quantitative sensory testing in the German Research Network on Neuropathic Pain (DFNS): somatosensory abnormalities in 1236 patients with different neuropathic pain syndromes. *Pain* **150**:439–450.

Meijer IA, Vanasse M, Nizard S, Robitaille Y, and Rossignol E (2014) An atypical case of SCN9A mutation presenting with global motor delay and a severe pain disorder. *Muscle Nerve* **49**:134–138.

Mert T and Gunes Y (2012) Antinociceptive activities of lidocaine and the nav1.8 blocker a803467 in diabetic rats. *J Am Assoc Lab Anim Sci* **51**:579–585.

Michiels JJ, te Morsche RH, Jansen JB, and Drenth JP (2005) Autosomal dominant erythermalgia associated with a novel mutation in the voltage-gated sodium channel alpha subunit Nav1.7. *Arch Neurol* **62**:1587–1590.

Payandeh J, Scheuer T, Zheng N, and Catterall WA (2011) The crystal structure of a voltage-gated sodium channel. *Nature* **475**:353–358.

Renganathan M, Cummins TR, and Waxman SG (2001) Contribution of Na(v)1.8 sodium channels to action potential electrogenesis in DRG neurons. *J Neurophysiol* **86**:629–640.

Rolke R, Baron R, Maier C, Tölle TR, Treede RD, Beyer A, Binder A, Birbaumer N, Birklein F, Bötefür IC, et al. (2006) Quantitative sensory testing in the German Research Network on Neuropathic Pain (DFNS): standardized protocol and reference values. *Pain* **123**:231–243.

Tanelian DL and Brose WG (1991) Neuropathic pain can be relieved by drugs that are use-dependent sodium channel blockers: lidocaine, carbamazepine, and mexiletine. *Anesthesiology* **74**:949–951.

Downloaded from molpharm.aspetjournals.org at ASPET Journals on January 13, 2020

Themistocleous AC, Crombez G, Baskozos G, and Bennett DL (2018) Using stratified medicine to understand, diagnose, and treat neuropathic pain. *Pain* **159** (Suppl 1): S31–S42.
Themistocleous AC, Ramirez JD, Shillo PR, Lees JG, Selvarajah D, Orengo C, Tesfaye S, Rice AS, and Bennett DL (2016) The Pain in Neuropathy Study (PiNS): a cross-sectional observational study determining the somatosensory phenotype of painful and painless diabetic neuropathy. *Pain* **157**:1132–1145.
Waxman SG, Merkies ISJ, Gerrits MM, Dib-Hajj SD, Lauria G, Cox JJ, Wood JN, Woods CG, Drenth JPH, and Faber CG (2014) Sodium channel genes in pain-related disorders: phenotype-genotype associations and recommendations for clinical use. *Lancet Neurol* **13**:1152–1160.
Yan Z, Zhou Q, Wang L, Wu J, Zhao Y, Huang G, Peng W, Shen H, Lei J, and Yan N (2017) Structure of the Nav1.4-β1 complex from electric eel. *Cell* **170**:470–482.e11.
Yang Y, Adi T, Effraim PR, Chen L, Dib-Hajj SD, and Waxman SG (2018) Reverse pharmacogenomics: carbamazepine normalizes activation and attenuates thermal hyperexcitability of sensory neurons due to Na_v 1.7 mutation I234T. *Br J Pharmacol* **175**:2261–2271.
Yang Y, Dib-Hajj SD, Zhang J, Zhang Y, Tyrrell L, Estacion M, and Waxman SG (2012) Structural modelling and mutant cycle analysis predict pharmacoresponsiveness of a $Na_{(V)}1.7$ mutant channel. *Nat Commun* **3**:1186.
Yang YC, Huang CS, and Kuo CC (2010) Lidocaine, carbamazepine, and imipramine have partially overlapping binding sites and additive inhibitory effect on neuronal Na+ channels. *Anesthesiology* **113**:160–174.

Address correspondence to: Dr. Sulayman D. Dib-Hajj, The Center for Neuroscience and Regeneration Research, VA Connecticut Healthcare System, 950 Campbell Avenue, Building 34, West Haven, CT 06516. E-mail: Sulayman.dib-hajj@yale.edu

Downloaded from molpharm.aspetjournals.org at ASPET Journals on January 13, 2020